Optimal trade-off filters for compressed Raman classification and spectrum reconstruction

Timothée Justel, Frédéric Galland, Antoine Roueff

Optimal tradeoff filters for compressed Raman classification and spectrum reconstruction

TIMOTHÉE JUSTEL[1], FRÉDÉRIC GALLAND[1,*], AND ANTOINE ROUEFF[2]

[1] Aix Marseille Univ, CNRS, Ecole Centrale Marseille, Institut Fresnel, Marseille, France.
[2] Université de Toulon, Aix Marseille Univ, CNRS, IM2NP, Toulon, France.
[*] Corresponding author: frederic.galland@fresnel.fr

Compiled April 18, 2023

Compressed Raman spectroscopy is a promising technique for fast chemical analysis. In particular, classification between species with known spectra can be performed with measures acquired through few binary filters. Moreover, it is possible to reconstruct spectra by using enough filters. As classification and reconstruction are competing, designing filters allowing to perform both tasks is challenging. To tackle this problem, we propose to build optimal tradeoff filters, i.e. filters so that there exist no filters achieving better performance both in classification and in reconstruction. With this approach, users get an overview of reachable performance and can choose the tradeoff most fitting their application.

http://dx.doi.org/10.1364/ao.XX.XXXXXX

1. INTRODUCTION

Spontaneous Raman scattering spectroscopy is a widely used technique to determine the chemical composition of a sample. However, the acquisition of a complete Raman spectrum with a standard spectrometer can be time-consuming hence incompatible with the constraints of some applications, in particular real-time analysis. This limitation is due to the low amount of photons generated by the Raman effect and to the fact that standard spectrometers make use of detector arrays, that are limited by electronic noise, to acquire the entire spectrum at once. Compressed Raman approaches have been developed to overcome this limitation. These approaches are based on counting the number of photons received on a small number of detectors of high sensitivity (i.e. that are only limited by photon noise) and high acquisition rate after filtering with binary filters designed to select the relevant frequencies of the Raman spectrum [1]. Such binary filters can be implemented e.g. using a digital micromirror device (DMD). It is possible to recover all spectral information from compressed measurements under certain conditions, e.g. when using sets of filters derived from the Hadamard basis [2–4] or when using a sufficient number of random filters [5–7]. However, when the spectra of sample species are known it is no longer necessary to reconstruct the entire spectrum in order to estimate their mixing coefficients or to perform a classification between the different species. Binary filters can be optimized to perform these tasks with few photons and few measurements [3, 8–15]. In particular, classification can be performed with a number of filters smaller than the number of species to discriminate [14, 16]. Nevertheless, such supervised compressed Raman approaches may lead to erroneous results for example if the sample contains unexpected species or in case of calibration drifts. It is therefore important to be able to check the actual spectra in case of doubt, in order to diagnose a problem or to update the a priori knowledge regarding the sample. Since performing additional measures is not always possible and would slow down the acquisition, thereby crippling the main advantage of compressed spectroscopy, it is important that this check be performed without requiring new measurements. In order to tackle this problem, it has been proposed in [16] to change filters at each pixel rather then always using the same binary filters optimized for classification. An example of such an acquisition system is shown in Fig. 1. By incurring a small loss in classification performance, this approach allows not only to perform classification at each pixel but also to reconstruct encountered spectra by combining measurements made on different pixels. This technique consists in building a large number of filters able to perform a reliable classification and select from this pool the combination of filters having the best reconstruction performance. In addition, classification and reconstruction performance are assessed using the Cramér-Rao bound, that provides a lower bound on the variance of any unbiased estimator, and the generalized Bhattacharyya bound [13], that upper-bounds the probability of classification error.

The algorithm proposed in [16] achieves a tradeoff between classification and reconstruction, but without guarantee of optimality. Moreover, this procedure lacks flexibility since it does not provide the user with fine control over the tradeoff, i.e to favor one task over the other. Indeed, other tradeoffs could have been interesting, e.g. being able to perform better classification by incurring a tolerable loss in reconstruction quality.

In this article, we propose a new and general methodology to address this multi-criteria optimization problem that relies on an optimal tradeoff filter approach [17–19]. In the considered setting, a combination of filters achieves an optimal tradeoff if there exists no other filter combination that performs both classification and reconstruction better. This corresponds to the notion of Pareto optimality whereas the set of optimal tradeoff filters corresponds to the Pareto frontier. We emphasize that filters that are not part of this set are strictly suboptimal since by definition there exists at least one other combination of filters that has better performance in both tasks. Besides, note that it is impossible to decide between two filter combinations achieving optimal tradeoffs without additional constraints since if one of them is better at one task then it is worse in the other. Hence filters should only be chosen amongst optimal tradeoff filters, e.g. distinguishing them by taking into account user-specific considerations such as a minimum targeted performance. Moreover, this methodology enables to fully characterize achievable classification / reconstruction performance, as we show on some examples below.

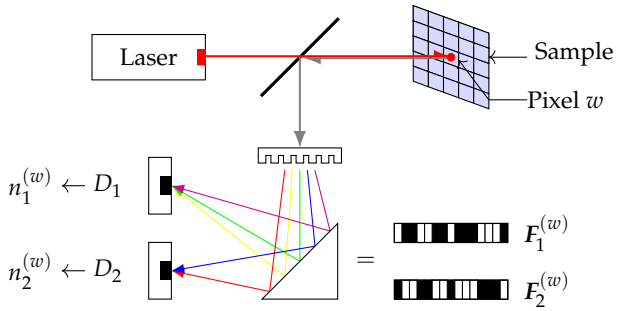

Fig. 1. Diagram of the acquisition system with $P = 2$ lossless and orthogonal filters applied in parallel.

2. COMPRESSED CLASSIFICATION AND SPECTRUM RECONSTRUCTION

We consider the same compressed Raman acquisition scheme as in [16] (see Fig. 1). On each pixel the Raman scattering radiation is measured through P lossless orthogonal binary filters (LOBF) applied in parallel [11, 20]. The set of filters used at pixel w is $\boldsymbol{F}^{(w)} = (\boldsymbol{F}_1^{(w)}, \dots, \boldsymbol{F}_P^{(w)})$ where $\boldsymbol{F}_m^{(w)} = (F_m^{(w)}(1), \dots, F_m^{(w)}(K))^T$ is the m^{th} filter of the set, P the number of filters, K the number of frequency bins and ^{T} the transpose. $F_m^{(w)}(k) \in \{0, 1\}$ is the binary filtering coefficient applied on the frequency range $[\nu_k - \delta_\nu/2, \nu_k + \delta_\nu/2]$. We assume that $\nu_{k+1} - \nu_k > \delta_\nu$, i.e. frequency bins are non-overlapping. Each of the filters is associated with a photon-counting detector D_m that is only limited by photon noise and with negligible electronic or readout noise [12]. Since filters are lossless and orthogonal, $\sum_{m=1}^{P} F_m^{(w)}(k) = 1$, i.e. at pixel w, for each frequency bin k, there exists one and only one filter m_0 among the P filters so that $F_{m_0}(k) = 1$, and thus $F_m(k) = 0$ for $m \neq m_0$ (see Fig. 1). This means that the photons in the k^{th} frequency bin are all redirected to the same detector (orthogonal filters), and cannot be redirected toward a rejection path (lossless filters[1]). We denote the number of photons received on D_m at pixel w through $\boldsymbol{F}_m^{(w)}$ by $n_m^{(w)}$. Let $\boldsymbol{S} = (S_1, \dots, S_K)^T$ be the normalized Raman spectrum appearing at pixel w (i.e. $\sum_{k=1}^{K} S_k = 1$). S_k corresponds to the average proportion of Raman scattering photons emitted in $[\nu_k - \delta_\nu/2, \nu_k + \delta_\nu/2]$. Let $\tau^{(w)}$ be the acquisition time at pixel w and $\gamma^{(w)}$ be the radiation intensity at w before filtering. The average number of photons measured by D_m at w then writes

$$\langle n_m^{(w)} \rangle = \tau^{(w)} \gamma^{(w)} \boldsymbol{F}_m^{(w)} \cdot \boldsymbol{S} \tag{1}$$

where $\langle\,\rangle$ is the statistical mean and $\cdot$ is the dot product. If a photon emitted by a species with a spectrum $\boldsymbol{S}$ is detected when performing measurements at pixel w, the probability that it is detected by D_m is $p_m^{(w)} = \langle n_m^{(w)} \rangle / \sum_{p=1}^{P} \langle n_p^{(w)} \rangle = \boldsymbol{F}_m^{(w)} \cdot \boldsymbol{S}$. Acquisition is stopped when the total number of detected photons reaches N, i.e. when $\sum_{m=1}^{P} n_m^{(w)} = N$. Fixing N rather than $\tau^{(w)}$ allows performance to be independent of $\gamma^{(w)}$ [14, 16]. Indeed, with this contraint, the measurement vector $\boldsymbol{n}^{(w)} = (n_1^{(w)}, \dots, n_P^{(w)})$ is distributed according to

$$\mathcal{P}(\boldsymbol{n}^{(w)} \mid \boldsymbol{S}, w) = N! \prod_{m=1}^{P} \frac{\left(p_m^{(w)}\right)^{n_m^{(w)}}}{n_m^{(w)}!}. \tag{2}$$

Assuming that the spectra of the M species appearing in the sample are known, it is possible to discriminate between them, even if $P < M$ [14]. If all species have the same probability to be observed at each pixel, the classifier minimizing the probability of classification error writes

$$\widehat{u}_{\text{opt}}^{(w)} = \underset{u}{\text{argmax}} \sum_{m=1}^{P} n_m^{(w)} \log p_m^{(w,u)} \tag{3}$$

where $p_m^{(w,u)}$ is the probability $p_m^{(w)}$ corresponding to the spectrum $\boldsymbol{S}^{(u)}$ of the species u. Its probability of error $\mathcal{P}(\epsilon^{(w)})$ is upper bounded by a generalized Bhattacharyya bound $\mathcal{B}^{(w)}$ [14]

$$\mathcal{P}(\epsilon^{(w)}) \leq \mathcal{B}^{(w)} = \frac{1}{M} \sum_{u} \sum_{v>u} \left(\sum_{m=1}^{P} \sqrt{p_m^{(w,u)} p_m^{(w,v)}} \right)^N. \tag{4}$$

As shown in [13, 14] minimizing this bound yields filter sets that allow one to discriminate between species reliably.

Conversely, reconstructing an unknown spectrum of size $K > P$ cannot be done using only the P measurements made with a single LOBF set without additional information. However, such a reconstruction can be performed from measures acquired from multiple pixels as soon as the corresponding combination of filter sets is a generating family of normalized spectra in $\mathbb{R}^K$. This implies that the minimum number of LOBF sets necessary to carry out reconstruction is $W_{\min} = \lceil \frac{K-1}{P-1} \rceil$. When $P = 2$ it is, for example, possible to use filter sets derived from the Hadamard S-matrix [2]. One can evaluate the reconstruction performance of a combination of filter sets using its Cramér-Rao bound (CRB). Indeed the CRB lower bounds the variance of any unbiased estimator [21]. Let σ_k^2 be the variance of any unbiased estimator of S_k; then

$$\sigma_k^2 \geq [\mathbf{Y}]_{k,k} = [\boldsymbol{I}_F^{-1}]_{k,k} \quad \forall k \in [\![1, K-1]\!] \tag{5}$$

where $\mathbf{Y}$ is the Cramér-Rao matrix, $\boldsymbol{I}_F$ is the Fisher information matrix (FIM) defined as $[\boldsymbol{I}_F]_{k,l} = -\langle \partial_{S_k} \partial_{S_l} \ell \rangle$ with $k, l \in [\![1, K-1]\!]$

[1] Note that in this paper, the term 'lossless' does not refer to the optical efficiency of the filters. We consider that optical losses due to acquisition system imperfections are directly embedded in the radiation intensity and the Raman spectrum.

and $\ell = \sum_{w=1}^{W} \log \mathcal{P}(\boldsymbol{n}^{(w)}|\boldsymbol{S}, w)$ the log-likelihood. Note that $k, l \in [\![1, K-1]\!]$ because $\boldsymbol{S}$ is normalized. From Eq. (2) we get [16]

$$[\boldsymbol{I}_F]_{k,l} = \sum_{w=1}^{W} N \sum_{m=1}^{P} \frac{\delta F_m^{(w)}(k)\, \delta F_m^{(w)}(l)}{\boldsymbol{F}_m^{(w)} \cdot \boldsymbol{S}} \tag{6}$$

where $\delta F_m(k) = F_m(k) - F_m(K)$. The trace of the CRB matrix $\operatorname{Tr} \mathbf{Y} = \sum_{k=1}^{K-1} [\mathbf{Y}]_{k,k}$ then provides a convenient criterion that can be used to select a combination of filter sets able to perform accurate reconstructions. In the following, since the spectrum to be estimated is unknown, we compute the CRB for the flat spectrum $S_k^{\text{flat}} = 1/K \ \forall k$ [16], but other solutions could be considered when information about the spectra to be reconstructed is available.

3. OPTIMAL TRADEOFF FILTERS

To extend the technique presented in [16], we are looking for optimal combinations of filters able to perform both classification and reconstruction. As explained above, supervised classification can be carried out from measurements made with a single set of filters $\boldsymbol{F}^{(w)}$. The classification performance of such a set can be measured with its Bhattacharyya bound $\mathcal{B}^{(w)}$ (see Eq. (4)). We choose to assess the classification performance of a combination of filters $\boldsymbol{F} = \{\boldsymbol{F}^{(1)}, \dots, \boldsymbol{F}^{(W)}\}$ (where W is the number of filter sets) with its average Bhattacharyya bound $\overline{\mathcal{B}} = \frac{1}{W} \sum_{w=1}^{W} \mathcal{B}^{(w)}$. On the other hand spectrum reconstruction can only be carried out from measurements made with a sufficient diversity of filter sets. We assess the reconstruction performance of a combination of filter sets $\boldsymbol{F}$ with the trace of its CRB matrix $\operatorname{Tr} \mathbf{Y}$.

Since $\overline{\mathcal{B}}$ and $\operatorname{Tr} \mathbf{Y}$ are competing one cannot minimize them simultaneously. A possibility to obtain sets of filters tailored for both tasks is to build a large pool of distinct sets able to perform classification reliably and then select the W sets of this pool leading to the best reconstruction performance [16]. However, a more general approach to this multi-criteria optimization problem exists, based on optimal tradeoff (OT) filters [17, 18].

$\boldsymbol{F}$ achieves an optimal tradeoff if no other filter combination performs uniformly better. Writing $\mathcal{F}_{\text{opt}}$ the set of OT filters,

$$\boldsymbol{F} \in \mathcal{F}_{\text{opt}} \Leftrightarrow \forall \boldsymbol{F}' \begin{cases} \overline{\mathcal{B}}(\boldsymbol{F}') \geq \overline{\mathcal{B}}(\boldsymbol{F}) \\ \quad \text{and/or} \\ \operatorname{Tr} \mathbf{Y}(\boldsymbol{F}') \geq \operatorname{Tr} \mathbf{Y}(\boldsymbol{F}). \end{cases} \tag{7}$$

In this article we look for OT filters amongst all combinations of filters comprising W LOBF sets of P filters. Any combination of filters that does not belong to the set of optimal tradeoff filters has at least one counterpart in $\mathcal{F}_{\text{opt}}$ that performs every task better.

This is illustrated in Fig. 2. The set of OT filters (blue diamonds) is located on the lower left edge of the set of reachable criteria, which appears as a blue curve. Points A and B correspond to optimal tradeoff filters, whereas C does not. C is obviously non-optimal because some points such as B are located at its bottom left hence perform uniformly better. It is impossible to decide between A and B on the basis of this graph. Indeed, A has better reconstruction performance than B but poorer classification performance.

The problem to test every combinations of filters including W sets of P filters of size K for optimality proved to be intractable in the considered setups. Rather, we follow [17] and look for OT filters minimizing the convex combination

$$\Psi(\lambda, \boldsymbol{F}) = (1-\lambda) \log \operatorname{Tr} \mathbf{Y}(\boldsymbol{F}) + \lambda \log \overline{\mathcal{B}}(\boldsymbol{F}). \tag{8}$$

It can be easily proved that combinations of filters minimizing $\Psi(\lambda, \boldsymbol{F})$ are part of $\mathcal{F}_{\text{opt}}$. However, the converse is not true, i.e it is possible that some optimal tradeoff filters do not correspond to any global minimum of Ψ. Indeed, the set of all filter combinations minimizing $\Psi(\lambda, \boldsymbol{F})$ for $\lambda \in [0, 1]$ is located on the convex hull of the set of reachable criteria in the space $(\log \operatorname{Tr} \mathbf{Y}, \log \overline{\mathcal{B}})$ (see appendix A). Fig. 2 shows a typical example of the difference between the OT filters (in blue) and the set of filter combinations minimizing Ψ (green circles). The convex hull appears as a dotted green curve, abusively called optimal tradeoff curve in the following. Although it is not possible to reach all OT filters by minimizing Ψ, minimization of this criterion usually yields a wide range of optimal tradeoff filters.

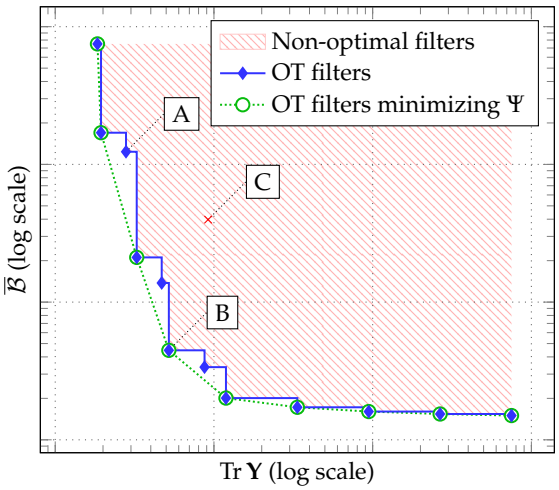

Fig. 2. Sketch of optimal tradeoff filters. The red area is the set of reachable criteria. Its interior corresponds to non-optimal filters. Its lower left edge (blue curve) corresponds to optimal tradeoff filters i.e. combinations of filters so that no other filter combination performs uniformly better. The green circles correspond to combinations of filters minimizing Ψ, which belong to the convex envelope of the set of OT filters.

Minimizing $\Psi(\lambda, \boldsymbol{F})$ is a challenging optimization problem owing to its non-convexity with respect to the filters $\boldsymbol{F}$, and the constraint $F_m^{(w)}(k) \in \{0, 1\}$. To tackle this problem we developed an optimization algorithm based on testing many successive random modifications from some starting filter combinations, the modifications being accepted only if they decrease $\Psi(\lambda, \boldsymbol{F})$ (see section B for details). Note that although such a computation is time-consuming it only has to be performed once, before acquisitions. The experiments of this article have been carried out with a procedure that should allow the discussion to be disturbed as little as possible by numerical issues. It outputs an optimal tradeoff curve in a few hours. In practice, it is possible to obtain a reasonable set of operating points in a matter of minutes using a lighter procedure (see section B).

4. EXAMPLES

In this section we illustrate the optimal tradeoff filters approach on a few examples. Considered spectra comprise $K = 128$ components and are randomly generated as $S_k^{(u)} =$

$(X_k^{(u)})^\alpha / \sum_{l=1}^{K} (X_l^{(u)})^\alpha$ where $X_k^{(u)}$ follows the exponential distribution with unit mean [13]. Here α is a "spikiness" parameter. If $\alpha = 1$ it is equivalent to draw $\boldsymbol{s}^{(u)}$ uniformly from the simplex of normalized spectra.

We first consider the case of the classification between $M = 3$ species whose spectra, drawn with $\alpha = 1$, are displayed on Fig. 3. In this example, it is assumed that only $P = 2$ detectors are used, which corresponds to the simplest situation to implement experimentally, and that $N = 250$ photons are acquired on each pixel. Moreover, the number of filter sets W is fixed to $W_{\min} = 127$, which corresponds to the size of the smallest region in which it is possible to reconstruct a spectrum [16]. Fig. 4 shows the optimal tradeoff curve computed using the algorithm of section B (blue curve). The W LOBF sets derived from the Hadamard S-matrix [2] also appear in the diagram (orange triangle). This combination of filter sets seems to minimize $\Psi(\lambda = 0, \boldsymbol{F})$ and thus has the best reconstruction performance of the curve, with $\operatorname{Tr} \mathbf{Y} = 3.9 \times 10^{-3}$. On the other hand, it also has the poorest classification performance. To compare with a simple baseline, points corresponding to 10^3 random LOBF set combinations are also shown on this graph (green disks). None of them are close to the optimal tradeoff curve, and they all have poor classification performance. The yellow crossed circle represents the W LOBF sets generated using the algorithm proposed in [16]. Although it is close to the optimal tradeoff curve it is not optimal. The red dashed horizontal line corresponds to the value of $\overline{\mathcal{B}}$ when using W times the same set of $P = 2$ filters optimized as proposed in [14]. The OT filters corresponding to the lower part of the curve have a slightly higher $\overline{\mathcal{B}}$ but allow reconstruction to be performed, which is not possible with a unique LOBF set when $P < K$.

It seems obvious that it is not relevant to optimize only one or the other criteria when aiming to realize both tasks, hence the interest of optimal tradeoff filters. The shape of the optimal tradeoff curve confirms this intuition. First, the lower part of the curve is nearly horizontal. This means that there are optimal tradeoff filters that allow for more accurate reconstruction than the one minimizing $\Psi(\lambda = 1, \boldsymbol{F})$ while having almost the same classification performance. For example, from $\lambda = 1$ to $\lambda = 0.75$ the trace of the CRB matrix varies from 96 to 0.1 whereas the average Bhattacharyya bound only varies from 2.4×10^{-4} to 2.9×10^{-4}. This loss of classification performance can be compensated by increasing N by only a factor of 1.02. Conversely, since $\operatorname{Tr} \mathbf{Y}$ is inversely proportional to N, it would take $N = 960 \times 250 = 2.4 \times 10^4$ detected photons for the OT filters minimizing $\Psi(\lambda = 1, \boldsymbol{F})$ to have the same reconstruction performance as the one minimizing $\Psi(\lambda = 0.75, \boldsymbol{F})$. The left part of the curve is steep, but not vertical. Nevertheless, a significant improvement of classification reliability compared to the topmost point can be achieved with a limited loss of reconstruction performance. In fact, from $\lambda = 0$ to $\lambda = 0.5$ the average Bhattacharyya bound varies from 0.73 to 1.3×10^{-3} whereas the trace of the CRB matrix varies from 3.9×10^{-3} to 1.7×10^{-2}. This loss of reconstruction performance can be counterbalanced by multiplying N by 4.3. On the other hand it would take more than 2.5×10^6 photons to the set minimizing $\Psi(\lambda = 0, \boldsymbol{F})$ to perform as well in classification as the one minimizing $\Psi(\lambda = 0.5, \boldsymbol{F})$. Hence it can be interesting to select OT filters located in the bend of the optimal tradeoff curve rather than close to its extremes.

We then consider the case of different triplets of spectra, each randomly drawn with different values of α. Fig. 5 shows the

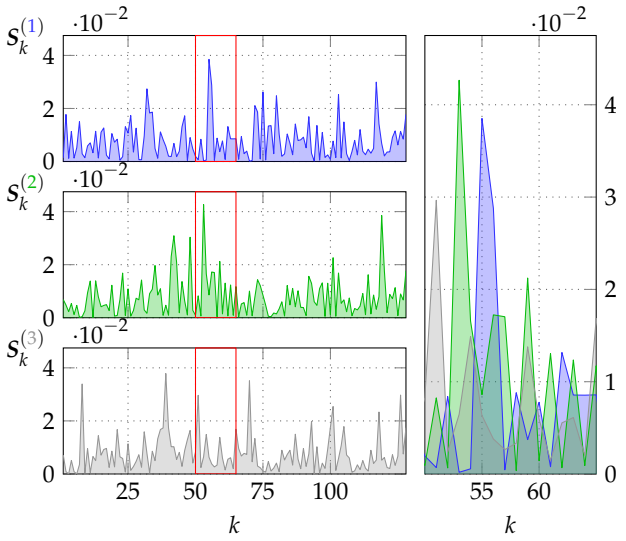

Fig. 3. Spectra to classify for the experiment of Fig. 4, randomly generated with $\alpha = 1$ (see text for details) and $K = 128$. Second column zooms over the frequency range highlighted in red.

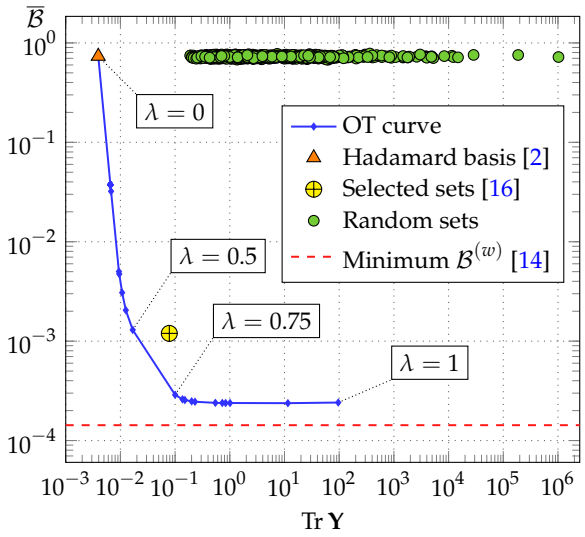

Fig. 4. Optimal tradeoff curve for $W = 127$ LOBF sets of $P = 2$ filters when $N = 250$ photons are detected on each pixel and for $M = 3$ species to discriminate. The spectra of these 3 species, generated with $\alpha = 1$ and $K = 128$, are shown in Fig. 3. The filter sets derived from the Hadamard S-matrix [2] and those generated as in [16] also appear on the graph. Bottom red line represents the $\mathcal{B}^{(w)}$ value of an LOBF set optimized as in [14]. Green disks correspond to 10^3 random combinations of filters.

$M = 3$ spectra generated with $\alpha = 0.5$ (top), $\alpha = 1$ (middle) and $\alpha = 2$ (bottom). Fig. 6 presents the optimal tradeoff curves computed for these spectra and, as before, combinations of filters comprising $W_{\min} = 127$ LOBF sets having $P = 2$ filters when there are $N = 250$ detected photons per pixel. Note that as the $M = 3$ spectra randomly generated for $\alpha = 1$ are different realizations in Fig. 4 and in Fig. 6 (blue curve), the optimized filters and the OT curves are also different. It appears clearly by comparing the position of the curves that the larger α is, the

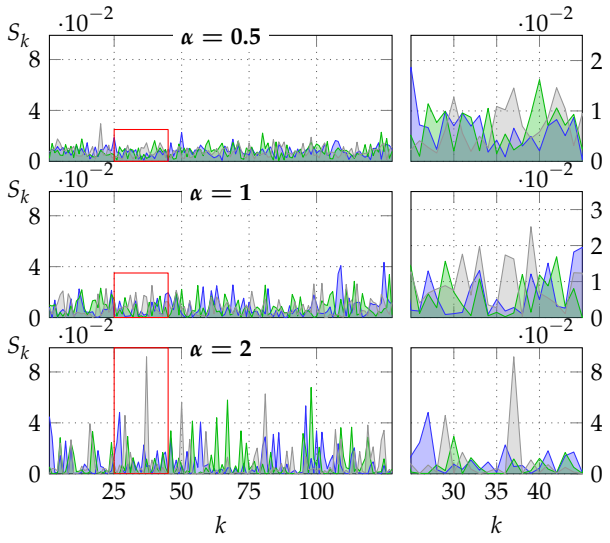

Fig. 5. Spectra to classify generated with different values of α for the experiment of Fig. 6 ($K = 128$). Second column zooms over the frequency range highlighted in red in the same row, first column.

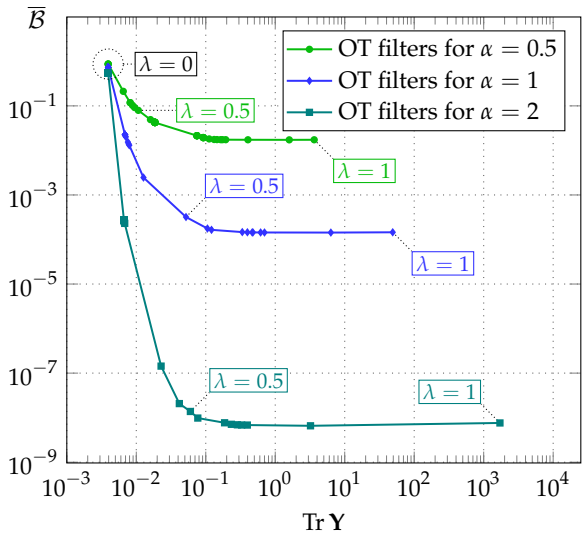

Fig. 6. Optimal tradeoff curves computed for discrimination between $M = 3$ spectra generated with different α and shown on Fig. 5. Results obtained for $W = 127$ LOBF sets of $P = 2$ filters when $N = 250$ photons are detected on each pixel.

easier spectra are to discriminate. In fact the lowest $\overline{\mathcal{B}}$ value reached with $\alpha = 0.5$ is 1.7×10^{-2} whereas it is 1.4×10^{-4} for $\alpha = 1$ and 9.8×10^{-9} for $\alpha = 2$. One can also note that the three curves almost begin from the same point. This is because $\Psi(\lambda, \boldsymbol{F})$ no more depends on $\overline{\mathcal{B}}$ when $\lambda = 0$, hence the OT filters minimizing $\Psi(\lambda = 0, \boldsymbol{F})$ do not depend on α. Furthermore, as in the previous case, the lower part of each curve is almost flat. Thus, in this example, it is possible to obtain better reconstruction performance than with the OT filters minimizing $\Psi(\lambda = 1, \boldsymbol{F})$ while having nearly the same classification performance. Conversely, the steepness of the left part of the optimal tradeoff curve depends on α, hence extra care has to be taken when analyzing the case of the OT filters minimizing $\Psi(\lambda = 0, \boldsymbol{F})$. Nonetheless, we emphasize that it is necessary in any case to go through the analysis of the optimal tradeoff curve to see which operating points are available for a given application. Such an analysis almost always leads to improved performance compared to the case where only one of the two criteria is optimized.

The third analyzed example is a more challenging case with $M = 5$ species to discriminate. The spectrum of each of these species is uniformly generated on the simplex of normalized spectra (i.e. with $\alpha = 1$). Fig. 7 shows the corresponding optimal tradeoff curves. The uppermost optimal tradeoff curve was computed for filter set combinations having the same parameters as before ($W = 127$, $P = 2$), for the same number of detected photons ($N = 250$) (see blue curve). While a variation of $\overline{\mathcal{B}}$ values of ~ 4 orders of magnitude could be observed between $\lambda = 0$ and $\lambda = 1$ in Fig. 4 for $M = 3$ species, there is only a variation of ~ 1 order of magnitude for $M = 5$ although spectra have still been generated with $\alpha = 1$. This curve also shows that such combination of filter sets have poor classification performance even when only the mean Bhattacharyya bound is optimized, i.e for $\lambda = 1$. In fact, $\overline{\mathcal{B}}$ stays above 0.1 all along the curve. Such performance can be not sufficient for some applications. To tackle this problem one possibility is to increase the number of detected photons N that triggers acquisition stop. The optimal tradeoff curve for combinations of filters having the same settings but with $N = 500$ appears in Fig. 7 as a light-green curve. Classification performance are greatly improved comparing to previous setup as it becomes possible to reach $\overline{\mathcal{B}}$ values around 10^{-2} while having reconstruction performance for which $\overline{\mathcal{B}}$ was about 0.1 when $N = 250$ (on the blue curve). However, doubling the number of detected photons implies doubling the mean measuring time. Another possibility that does not increase the acquisition time is to increase P, i.e. increase the number of parallel measurements per pixel.

The dark-green curve of Fig. 7 is the optimal tradeoff curve drawn for combinations of filters including $W = 127$ sets of filters having (unlike before) $P = 3$ filters, when the number of photons detected per pixel is $N = 250$. With this configuration $\overline{\mathcal{B}}$ values lower than 10^{-4} can be achieved for Tr $\mathbf{Y}$ values for which the $\overline{\mathcal{B}}$ was about 10^{-2} when $N = 500$ and $P = 2$ (on the light green curve). Hence, although using 3 filters (hence 3 detectors) instead of 2 significantly complexifies the imaging system it can be interesting due to the significant performance gain that results. One can also note that there exist some OT filters having $P = 3$ filters that perform uniformly better than any combination of filter sets having $P = 2$ filters for $N = 250$ (see red rectangle in Fig. 7).

5. CONCLUSION

In this article we propose to use the optimal tradeoff filters approach to build binary filters able to perform both classification and spectrum reconstruction in a compressed Raman setup. To build these filters we minimize a convex combination of the two criteria assessing filters performance, namely the generalized Bhattacharyya bound and the trace of the Cramér-Rao bound. This allows us to find filters on the convex hull of the set of optimal tradeoff filters, amongst which the user has to choose. Another interest of drawing the optimal tradeoff curve is to get an overview of reachable criteria for given parameters and to measure the impact of their modification on performance. Such an approach hence provides appropriate tools for building and choosing the filter set combination to use for measurements.

One straightforward perspective is to implement the ap-

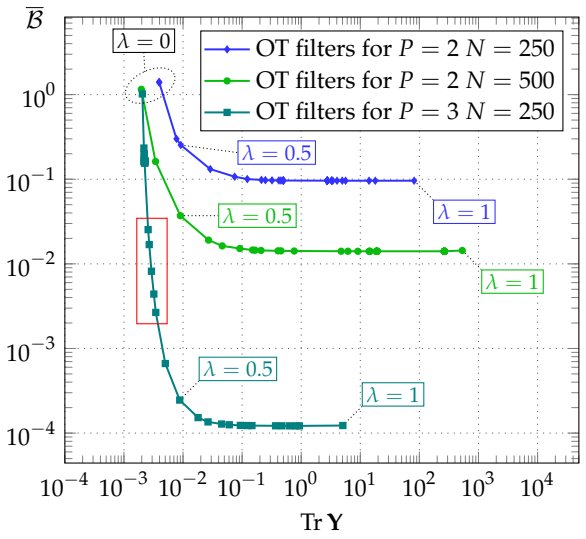

Fig. 7. Optimal tradeoff curves optimized for discrimination between $M = 5$ spectra generated with $\alpha = 1$ and $K = 128$. Results obtained for $W = 127$ LOBF sets of $P = 2$ or $P = 3$ filters when $N = 250$ or 500 photons are detected on each pixel. Optimal tradeoff filters inside the red rectangle perform uniformly better than any combination of filters of the curve drawn for $P = 2$, $N = 250$.

proach on a real experimental setup. Since performing both classification and reconstruction opens up the possibility to question or update the a priori knowledge regarding the sample, the development of corresponding methods also seems a logical continuation of this work. In particular, the next challenge is to investigate the best way to incorporate a null class during the classification process - i.e. a class for spectra that are distinct from the references. Binary filters are widely used as they can be easily implemented using a digital micromirror device. It would nevertheless be interesting to extend the analysis to non-binary filters. It would also allow to quantitatively analyze the impact of filter binarity on performance. Moreover, in this paper, we only considered the case of classification, i.e. it is assumed that each pixel contains a single species. The generalization of the proposed approach to a mixture of species is thus another challenge.

A. CONVEXITY OF THE OPTIMAL TRADEOFF CURVE

The optimal tradeoff curve corresponds to the combinations of filters minimizing $\Psi(\lambda, \boldsymbol{F})$ for $\lambda \in [0,1]$. In this section we show that this curve is located on the convex hull of the set of reachable criteria in the space $(\log \mathrm{Tr}\, \mathbf{Y}, \log \overline{\mathcal{B}})$. Let $\boldsymbol{F}_\lambda = \mathrm{argmin}_{\boldsymbol{F}}\, \Psi(\lambda, \boldsymbol{F})$. Let also $\boldsymbol{F}$ and $\boldsymbol{F}'$ be so that $\log \mathrm{Tr}\, \mathbf{Y}(\boldsymbol{F}) \leq \log \mathrm{Tr}\, \mathbf{Y}(\boldsymbol{F}_\lambda) \leq \log \mathrm{Tr}\, \mathbf{Y}(\boldsymbol{F}')$. Then, there exists $\mu \in [0,1]$ such that

$$\log \mathrm{Tr}\, \mathbf{Y}(\boldsymbol{F}_\lambda) = \mu \log \mathrm{Tr}\, \mathbf{Y}(\boldsymbol{F}) + (1-\mu) \log \mathrm{Tr}\, \mathbf{Y}(\boldsymbol{F}'). \quad \textbf{(9)}$$

Moreover, by definition

$$\Psi(\lambda, \boldsymbol{F}_\lambda) \leq \Psi(\lambda, \boldsymbol{F}) \text{ and } \Psi(\lambda, \boldsymbol{F}_\lambda) \leq \Psi(\lambda, \boldsymbol{F}')$$

thus

$$\Psi(\lambda, \boldsymbol{F}_\lambda) \leq \mu \Psi(\lambda, \boldsymbol{F}) + (1-\mu) \Psi(\lambda, \boldsymbol{F}').$$

Using Eq. (9) we have

$$\begin{aligned}&(1-\lambda) \log \mathrm{Tr}\, \mathbf{Y}(\boldsymbol{F}_\lambda) + \lambda \log \overline{\mathcal{B}}(\boldsymbol{F}_\lambda) \\ &\leq (1-\lambda) \log \mathrm{Tr}\, \mathbf{Y}(\boldsymbol{F}_\lambda) + \lambda(\mu \log \overline{\mathcal{B}}(\boldsymbol{F}) + (1-\mu) \log \overline{\mathcal{B}}(\boldsymbol{F}')),\end{aligned}$$

hence,

$$\log \overline{\mathcal{B}}(\boldsymbol{F}_\lambda) \leq \mu \log \overline{\mathcal{B}}(\boldsymbol{F}) + (1-\mu) \log \overline{\mathcal{B}}(\boldsymbol{F}')$$

i.e. the optimal tradeoff curve is located on the convex hull of the set of reachable criteria in the space $(\log \mathrm{Tr}\, \mathbf{Y}, \log \overline{\mathcal{B}})$.

B. OPTIMIZATION ALGORITHM

This section provides details about the algorithm used to draw the optimal tradeoff curve. By definition, this means finding the combinations of filters comprising W LOBF sets of P filters that minimize $\Psi(\lambda, \boldsymbol{F}) = (1-\lambda) \log \mathrm{Tr}\, \mathbf{Y} + \lambda \log \overline{\mathcal{B}}$ for λ in $[0,1]$. This criterion is non-convex with respect to filters. Moreover, the set of all binary filters is discrete. Our algorithm is based on successive random modifications of combinations of LOBF sets, accepted only when they decrease the criterion. In order to explore a reasonable part of the filters space in a reasonable amount of time, efforts has been made to speed up criterion computation. In the following we start with a detailed description of the algorithm, and leave criterion computation matters to section C.

The following procedure is applied at fixed λ. The algorithm is given an initial combination of filters. Each step consists in testing one random modification of the current filter set combination. First, a set index w and a frequency bin index k are drawn uniformly from available indices. A new vector $(F_1^{(w)}(k), \ldots, F_P^{(w)}(k))$ is then uniformly drawn from authorized values. If it strictly increases the value of $\Psi(\lambda, \boldsymbol{F})$ for the current λ the change is rejected and it is forbidden to try it again. Because we are only looking for filters able to perform both classification and estimation, the Fisher information matrix has to remain invertible after each modification. Hence a change is also rejected (and forbidden) if the resulting filter set combination has a singular FIM. Note that this contraint is even applied when $\lambda = 1$, i.e. when only the mean Bhattacharyya bound is optimized. If the modification decreases the criterion and preserves FIM invertibility it is accepted and the list of forbidden changes is reset. The algorithm stops either when it reaches the maximum number of iterations or because any possible modification increases the criterion.

In order to explore more space and to be less susceptible to local minima, the whole process is repeated from multiple starting points for each λ. Only the trial resulting in the minimum value of $\Psi(\lambda, \boldsymbol{F})$ is kept. Moreover since trials do not depend on each other it is possible to run them in parallel on multiple CPU cores. For the experiments presented in this article we use 16 starting points for each value of λ. Twelve of these starting points are constituted of W random LOBF sets uniformly drawn for each λ until their FIM becomes invertible (which is usually the case within few draws). If $P = 2$ the 13^{th} starting point is constituted of filters derived of the Hadamard S-matrix [2] (else it is also random). The 14^{th} is constituted of filters optimized with the algorithm described in [16], except that selection is done in order to minimize $\overline{\mathcal{B}}$ and not Tr $\mathbf{Y}$ (but still enforcing FIM invertibility). This point is usually located next to the end of the optimal tradeoff curve, and is common to all λ. The two last starting points are filter set combinations optimized by the algorithm for the

two values of λ neighbouring the current one (if available, else they are random).

The choice of λ values is not straightforward. In fact the relationship between their localization in $[0,1]$ and the localization of the operating points found by the algorithm in the $(\log \mathrm{Tr}\,\mathbf{Y}, \log \overline{\mathcal{B}})$ space is difficult to anticipate. Moreover, as can be seen in section 4, the two criteria can vary of orders of magnitude along the curve. This means that great variations of their relative values occur within optimization. We observed that applying the logarithm on both criteria mitigates this problem, usually leading to a better sampling of the curve. With $\Psi(\lambda, \boldsymbol{F})$ comprising logarithms as in Eq. (8) a linear slicing of $[0,1]$ is generally sufficient to obtain reasonably well distributed operating points. It is nonetheless possible to improve curve sampling by using a dynamic λ range. The experiments shown in section 4 implement the following heuristic. The first two λ values are 0 and 1. Let $\boldsymbol{F}_{\lambda_1}$ and $\boldsymbol{F}_{\lambda_2}$ be the OT filters found by the algorithm that are the furthest apart in the sense of the 2-norm in the $(\log \mathrm{Tr}\,\mathbf{Y}, \log \overline{\mathcal{B}})$ plane. Then, the next λ value used by the algorithm is $(\lambda_1 + \lambda_2)/2$.

Computing the curve of Fig. 4 took few hours. All trials ran in parallel and there was no limitation over the maximum number of iterations, in order for the results presented in this article not to be disturbed too much by numerical issues. In practice, it is possible to reduce computation time by limiting the number of iterations or the number of trials. Fig. 8 compares the curve of Fig. 4 with another curve obtained for the same example with a lighter optimization procedure. This procedure comprises a unique trial, starting for each λ from last optimized sets. Hence the corresponding optimal tradeoff curve is drawn iteratively. The number of iterations is limited to 10^4 and λ values are linearly distributed between 0 and 1 with a step size of 2.5×10^{-2}. With such restrictions the computing time is approximately 5 minutes per curve. The procedure is applied twice, from two different starting points, namely the filter sets derived from the Hadamard basis and the sets optimized in terms of $\overline{\mathcal{B}}$ with the variation of the algorithm of [16]. The curve appearing in light green in Fig. 8 is the convex hull of these two curves in the $(\log \mathrm{Tr}\,\mathbf{Y}, \log \overline{\mathcal{B}})$ space. In this example, using operating points from this curve rather than the curve obtained with the full optimization procedure only leads to a limited loss of performance. Nonetheless, one should note that there is no guarantee that the performance loss be limited in general. However considering the extreme reduction in computing time, it is interesting to compute this suboptimal curve beforehand in order to have a first set of reasonable operating points.

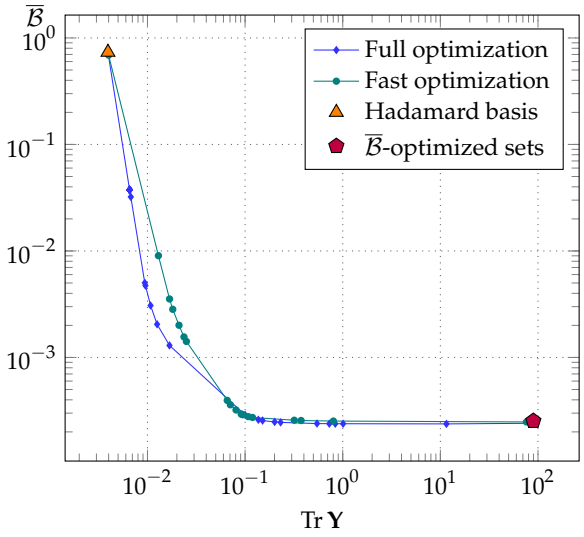

Fig. 8. Optimal tradeoff curves for $K = 128$, $P = 2$, $M = 3$ and $N = 250$. The curve labelled "full optimization" was drawn with the standard optimization procedure. The other curve was generated with a simplified procedure, in particular with a maximum of 10^4 iterations.

C. FAST COMPUTATION OF THE CRITERIA

The algorithm presented in section B is based on testing a large number of successive random modifications of LOBF sets. In the simulations appearing in this article for $P = 2$, $K = 128$ and $W = 127$ the mean number of iterations necessary for the algorithm to converge is about 5×10^5 per trial. Moreover, increasing P or K greatly raises the number of iterations before converging. It is then critically important to compute criteria quickly.

Recall that $\overline{\mathcal{B}} = \frac{1}{W} \sum_{w=1}^{W} \mathcal{B}^{(w)}$ with $\mathcal{B}^{(w)}$ depending only on $\boldsymbol{F}^{(w)}$. Since filter sets are modified one at a time, it is possible to re-compute only one of the W terms of this sum at each step of the algorithm. Even if it is also the case for the FIM, one has to invert it at each step to get the Cramér-Rao matrix. Given the fact that this matrix is of size $(K-1) \times (K-1)$ this operation is a clear computational bottleneck. Let $\boldsymbol{I}_F^{(t)}$ be the FIM at the end of the t^{th} step of the algorithm. It is possible to write $\boldsymbol{I}_F^{(t)}$ as a function of $\boldsymbol{I}_F^{(t-1)}$ such that it is possible to take advantage of the Woodbury matrix identity to reduce the cost of computing the CRB. This identity states in particular that if $\boldsymbol{A}$, $\boldsymbol{B}$, $\boldsymbol{U}$, $\boldsymbol{V}$ are matrices of the right size and if $\boldsymbol{A}$, $\boldsymbol{B}$ and $\boldsymbol{A} + \boldsymbol{U}\boldsymbol{B}^{-1}\boldsymbol{V}$ are invertible then

$$\left[\boldsymbol{A} + \boldsymbol{U}\boldsymbol{B}^{-1}\boldsymbol{V}\right]^{-1} = \boldsymbol{A}^{-1} - \boldsymbol{A}^{-1}\boldsymbol{U}\left[\boldsymbol{B} + \boldsymbol{V}\boldsymbol{A}^{-1}\boldsymbol{U}\right]^{-1}\boldsymbol{V}\boldsymbol{A}^{-1}.$$

Let v and ℓ respectively be the index of the set and of the frequency bin modified in step t. Recall that step t consists in drawing a new value of $(F_1^{(v)}(\ell), \ldots, F_P^{(v)}(\ell))$. Since filters are lossless and orthogonal there is a unique m for which $F_m^{(w)}(k) = 1$ hence there are only two filter coefficients $F_i^{(v)}(k)$ and $F_j^{(v)}(k)$ that are modified within step t. Since

$$[\boldsymbol{I}_F]_{k,l} = \sum_{w=1}^{W} N \sum_{m=1}^{P} \frac{\delta F_m^{(w)}(k)\, \delta F_m^{(w)}(l)}{\boldsymbol{F}_m^{(w)} \cdot \boldsymbol{S}}$$

we have

$$\left[\boldsymbol{I}_F^{(t)}\right]_{k,l} = \left[\boldsymbol{I}_F^{(t-1)}\right]_{k,l} + \sum_{m \in \{i,j\}} \left[\frac{N\, \delta F_m^{(v,t)}(k)\, \delta F_m^{(v,t)}(l)}{\boldsymbol{F}_m^{(v,t)} \cdot \boldsymbol{S}} - \frac{N\, \delta F_m^{(v,t-1)}(k)\, \delta F_m^{(v,t-1)}(l)}{\boldsymbol{F}_m^{(v,t-1)} \cdot \boldsymbol{S}} \right].$$

It is then possible to write

$$\boldsymbol{I}_F^{(t)} = \boldsymbol{I}_F^{(t-1)} + \boldsymbol{U}_t\, \boldsymbol{B}_t^{-1}\, \boldsymbol{U}_t^T$$

with

$$\boldsymbol{U}_t = \left(\delta \boldsymbol{F}_i^{(v,t)} \,|\, \delta \boldsymbol{F}_j^{(v,t)} \,|\, \delta \boldsymbol{F}_i^{(v,t-1)} \,|\, \delta \boldsymbol{F}_j^{(v,t-1)}\right)$$

$$\boldsymbol{B}_t = \frac{1}{N} \mathrm{Diag}\left(\boldsymbol{F}_i^{(v,t)} \cdot \boldsymbol{S},\, \boldsymbol{F}_j^{(v,t)} \cdot \boldsymbol{S},\, -\boldsymbol{F}_i^{(v,t-1)} \cdot \boldsymbol{S},\, -\boldsymbol{F}_j^{(v,t-1)} \cdot \boldsymbol{S}\right),$$

where $(\boldsymbol{A}|\boldsymbol{B})$ is the concatenation of $\boldsymbol{A}$ and $\boldsymbol{B}$ and $\mathrm{Diag}(\boldsymbol{A})$ is the diagonal matrix whose diagonal values are the elements of the vector $\boldsymbol{A}$. Hence the CRB matrix can be written as

$$\mathbf{Y}^{(t)} = \mathbf{Y}^{(t-1)} - \left[\mathbf{Y}^{(t-1)}\boldsymbol{U}_t\right]\left[\boldsymbol{B}_t + \boldsymbol{U}_t^T\,\mathbf{Y}^{(t-1)}\boldsymbol{U}_t\right]^{-1}\left[\boldsymbol{U}_t^T\,\mathbf{Y}^{(t-1)}\right],$$

which only requires to invert a 4×4 matrix. Moreover,

$$\mathrm{Tr}\,\mathbf{Y}^{(t)} = \mathrm{Tr}\,\mathbf{Y}^{(t-1)} + \mathrm{Tr}\left(\left[\boldsymbol{B}_t + \boldsymbol{U}_t^T\,\mathbf{Y}^{(t-1)}\boldsymbol{U}_t\right]^{-1}\left[\boldsymbol{U}_t^T\,\mathbf{Y}^{(t-1)}\right]\left[\mathbf{Y}^{(t-1)}\boldsymbol{U}_t\right]\right),$$

which is even faster owing to the new order of matrix products.

Funding. France 2030 investment plan managed by the French National Research Agency (ANR-21-ESRE-0002).

Acknowledgments. We thank Philippe Réfrégier for advising us to analyse the optimal tradeoffs. We also thank Clément Grand and Hervé Rigneault for fruitful discussions.

Disclosures. The authors declare no conflicts of interest.

Data availability. Data underlying the results presented in this paper are not publicly available at this time but may be obtained from the authors upon reasonable request.

REFERENCES

1. D. Cebeci, B. R. Mankani, and D. Ben-Amotz, "Recent trends in compressive raman spectroscopy using dmd-based binary detection," J. Imaging **5**, 1 (2019).
2. R. A. DeVerse, R. M. Hammaker, and W. G. Fateley, "Realization of the hadamard multiplex advantage using a programmable optical mask in a dispersive flat-field near-infrared spectrometer," Appl. Spectrosc. **54**, 1751–1758 (2000).
3. B. M. Davis, A. J. Hemphill, D. Cebeci Maltaş, M. A. Zipper, P. Wang, and D. Ben-Amotz, "Multivariate hyperspectral raman imaging using compressive detection," Anal. chemistry **83**, 5086–5092 (2011).
4. P. Berto, C. Scotté, F. Galland, H. Rigneault, and H. B. de Aguiar, "Programmable single-pixel-based broadband stimulated raman scattering," Opt. letters **42**, 1696–1699 (2017).
5. D. F. Galvis-Carreño, Y. H. Mejía-Melgarejo, and H. Arguello-Fuentes, "Efficient reconstruction of raman spectroscopy imaging based on compressive sensing," Dyna **81**, 116–124 (2014).
6. J. V. Thompson, J. N. Bixler, B. H. Hokr, G. D. Noojin, M. O. Scully, and V. V. Yakovlev, "Single-shot chemical detection and identification with compressed hyperspectral raman imaging," Opt. letters **42**, 2169–2172 (2017).
7. F. Soldevila, J. Dong, E. Tajahuerce, S. Gigan, and H. B. de Aguiar, "Fast compressive raman bio-imaging via matrix completion," Optica **6**, 341–346 (2019).
8. D. Wilcox, G. Buzzard, B. Lucier, P. Wang, and D. Ben-Amotz, "Photon level chemical classification using digital compressive detection," Anal. chimica acta **755**, 17–27 (2012).
9. D. Wilcox, G. Buzzard, B. Lucier, O. Rehrauer, P. Wang, and D. Ben-Amotz, "Digital compressive chemical quantitation and hyperspectral imaging," The Analyst **138** (2013).
10. O. G. Rehrauer, B. R. Mankani, G. T. Buzzard, B. J. Lucier, and D. Ben-Amotz, "Fluorescence modeling for optimized-binary compressive detection raman spectroscopy," Opt. Express **23**, 23935–23951 (2015).
11. P. Réfrégier, C. Scotté, H. B. de Aguiar, H. Rigneault, and F. Galland, "Precision of proportion estimation with binary compressed raman spectrum," J. Opt. Soc. Am. A **35**, 125–134 (2018).
12. C. Scotté, H. B. de Aguiar, D. Marguet, E. M. Green, P. Bouzy, S. Vergnole, C. P. Winlove, N. Stone, and H. Rigneault, "Assessment of compressive raman versus hyperspectral raman for microcalcification chemical imaging," Anal. chemistry **90**, 7197–7203 (2018).
13. P. Réfrégier and F. Galland, "Bhattacharyya bound for raman spectrum classification with a couple of binary filters," Opt. Lett. **44**, 2228–2231 (2019).
14. P. Réfrégier, E. Chevallier, and F. Galland, "Compressed Raman classification method with upper-bounded error probability," Optics Letters **44**, 5836 (2019).
15. C. Scotté, S. Sivankutty, R. A. Bartels, and H. Rigneault, "Line-scan compressive raman imaging with spatiospectral encoding," Opt. Lett. **45**, 5567–5570 (2020).
16. T. Justel, F. Galland, and A. Roueff, "Compressed raman method combining classification and estimation of spectra with optimized binary filters," Opt. Lett. **47**, 1101–1104 (2022).
17. P. Réfrégier, "Filter design for optical pattern recognition: multicriteria optimization approach," Opt. Lett. **15**, 854–856 (1990).
18. P. Réfrégier, "Optimal trade-off filters for noise robustness, sharpness of the correlation peak, and horner efficiency," Opt. Lett. **16**, 829–831 (1991).
19. J. Figue and P. Réfrégier, "Optimality of trade-off filters," Appl. optics **32**, 1933–1935 (1993).
20. O. G. Rehrauer, V. C. Dinh, B. Mankani, G. Buzzard, B. Lucier, and D. Ben-Amotz, "Binary complementary filters for compressive raman spectroscopy," Appl. Spectrosc. **72**, 69 – 78 (2018).
21. P. H. Garthwaite, I. T. Jolliffe, and B. Jones, *Statistical Inference* (Wiley, 2002), 2nd ed.